Superradiance of polaritons: Crossover from two-dimensional to three-dimensional crystals

V. M. Agranovich, D. M. Basko, and O. A. Dubovsky

Citation: The Journal of Chemical Physics **106**, 3896 (1997); doi: 10.1063/1.473104
View online: http://dx.doi.org/10.1063/1.473104
View Table of Contents: http://scitation.aip.org/content/aip/journal/jcp/106/10?ver=pdfcov
Published by the AIP Publishing

Superradiance of polaritons: Crossover from two-dimensional to three-dimensional crystals

V. M. Agranovich, D. M. Basko, and O. A. Dubovsky
Institute for Spectroscopy, Russian Academy of Sciences, Troitsk, Moscow Obl. 142092, Russian Federation

(Received 3 July 1996; accepted 5 November 1996)

In spite of the relative simplicity of the structure of Frenkel excitons in molecular crystals some questions concerning the theory of polaritons in such crystals remain controversial—especially those concerning the crossover from the two-dimensional to the three-dimensional case. In the present work a detailed microscopic study of Frenkel exciton-polaritons in crystal slabs of arbitrary thickness is performed for the states with the tangential wave vector $\mathbf{k}_{\|}=0$. Starting from the microscopic quantum theory we have obtained two basic equations. One of them relates the complex energy of a polariton E to the quantity q, which in the limiting case of bulk crystal comes to the normal component of the wave vector. When the number N of the monolayers in the pile is large, $N\gg 1$, this equation is reduced to the dispersion equation of the macroscopic electrodynamics which uses the dielectric function $\epsilon(\omega)$. The other equation of our microscopic theory has the meaning of Ewald's extinction rule and for $N\gg 1$ is reduced to Maxwell's boundary conditions. Using the equations obtained we found the complete set of polariton terms for the arbitrary N from $N=1$ to $N\to\infty$. We have traced the rise and evolution of two branches of polariton terms with increasing N. Special attention was paid to the study of polariton superradiance—enormous radiative damping or very short corresponding lifetimes for some states. At small $N\ll\lambda/a$, with λ being the light wavelength and a the lattice constant, the superradiant linewidth is proportional to $N(\lambda/a)^2\Gamma^{(0)}$, where $\Gamma^{(0)}$ is the molecular radiative width. After further increasing the thickness this linewidth is monotonously decreased to zero. We also show that for the macroscopic slabs the radiative broadening may be obtained as a result of taking into account multiple reflections of the polariton from the surfaces of the crystal. Illustrative calculations were performed using parameters of the anthracene crystal. [S0021-9606(97)52106-4]

I. INTRODUCTION

Polaritons in infinite three-dimensional (3D) crystals have no radiative width and the decay of these elementary excitations may be caused by imperfections of a crystal lattice or interactions with other elementary excitations (phonons, etc.).[1,2] However, in crystals of lower dimensionality, i.e., in one-dimensional (1D) and two-dimensional (2D) crystals, the situation is different. In these cases, along with the polariton states which have no radiative width, there are polariton branches whose radiative width is enormous, i.e., of the order of $\Gamma^{(0)}(\lambda/2\pi a)$ for 1D crystals and $\Gamma^{(0)}(\lambda/2\pi a)^2$ for 2D crystals, with $\Gamma^{(0)}$ being the radiative width for an isolated molecule, k the polariton wave vector, and a the lattice constant.[3,4] The factor λ/a for 1D crystal and $(\lambda/a)^2$ for 2D crystal has a simple physical meaning—it is determined by the number of molecules in the so-called cooperative volume λ^D, which oscillate approximately in phase (here λ is the light wavelength and D is the dimensionality).

The first experimental studies of polaritons in low-dimensional crystal were performed for Frenkel excitons in molecular crystals of anthracene, where nature itself has taken care of the creation of appropriate 2D structures. For the lowest singlet electronic excitation in an anthracene molecule the wavelength $\lambda=400$ nm and $\Gamma^{(0)}=2\times10^8\ \mathrm{s}^{-1}$. This means that for an isolated monolayer of anthracene molecules (with lattice constants $a_1=6$ Å, $a_2=8$ Å) one may expect the radiative width $\Gamma^{(2)}\sim\Gamma^{(0)}(\lambda/2\pi a)^2\sim10^{12}\ \mathrm{s}^{-1}$, which corresponds to the lifetime $\tau=1/\Gamma^{(2)}\sim1$ ps. Such an increase in the radiative width is now commonly called ''superradiance.'' It was first observed by Aaviksoo, Lippmaa, and Reino[5] in the outermost monolayer of anthracene crystals. It is well known that the lowest electronic excitation energy of this monolayer the (2D exciton state) in anthracene is blueshifted by 204 cm^{-1} with respect to the excitation of the bulk. Hence, the electronic transition energy in the first monolayer lies between the bulk value and that for an isolated molecule which is blueshifted by 2000 cm^{-1} with respect to the bulk. The excited electronic state of this surface monolayer is clearly seen in the emission spectra at low temperatures. The excitations in the next-to-the-surface monolayer are blueshifted by 10 cm^{-1} and in the following one by 2 cm^{-1} with respect to the bulk. The nature of these blueshifts is well understood as being due to the absence of neighbors for the molecules in the outermost monolayer and the change in the value of the solvent shift. At low temperatures the surface layer acts as an isolated monolayer and is an appropriate system for studying 2D excitons. In Ref. 5 the measurements of the superradiant decay were carried out by means of a time-resolved technique. Measurements of the relative quantum yield of the bulk and surface emission indicated that the decay of the monolayer exciton is mainly radiative with a small contribution of the relaxation to the bulk. The picosecond relaxation time scales observed in

these experiments were a first example of superradiance in a two-dimensional excitonic system.

A second example of enhanced radiative recombination of two-dimensional excitons was given more recently by Devead *et al.*[6] in a high quality single quantum well (QW). Enhanced radiative recombination of the excitons (2D Wannier–Mott excitons in this case) revealed by a short lifetime (10 ± 4 ps) as well as by strong intensity of the signal is in agreement with the theory. We now observe intensive studies of enhanced radiative recombination of excitons in semiconductor QWs.

Several attempts were made to study the polariton spectra of these crystal slabs with arbitrary thickness, which is the intermediate situation between 2D and 3D (bulk) crystal. A solution to this problem has to expose the continuous transition from superradiant 2D polariton spectra to nonradiative spectra of polaritons in 3D crystals.

The phenomenological classical theory using the dielectric function $\varepsilon(\omega)$ was developed by Kliever and Fuchs.[7] This theory is valid for slab thicknesses far exceeding the distance a between the monolayers and for large wavelengths, $\lambda \gg a$. Our results are in agreement with those obtained by Philpott for crystal slabs of oscillating dipoles.[8] However, in that paper the problem of polariton radiative widths was not treated at all. The quantum mechanical microscopic approach was used by Knoester.[9,10] In these works the off-diagonal elements in the radiative self-energy were neglected and pole approximations were used (for a more detailed discussion see Sec. II). In these works the oscillating dependence of the radiative width of the excitonlike polaritons with the lowest energy on the crystal thickness (or the number of monolayers N) was found. This approach was developed by Björk *et al.*,[11] who did not use pole approximations. We avoid the simplifications mentioned above and our result does not show oscillations for large N. The same conclusion was made by Andreani,[12] who used the macroscopic approach.

The microscopic quantum theory of Frenkel exciton–polaritons in crystal slabs of arbitrary thickness is developed in the present work without these simplifications. Along with the complex energy E of a polariton, in our theory a new quantity q appears in a natural way, which for macroscopic slabs (large N) has the sense of a normal-to-the-slab plane component of a wave vector. We will refer to it as a wave vector at any N, but imply the meaning mentioned above. We found a new dispersion equation for the polariton energy E and q which is invariant under transformation $q \rightarrow q + 2\pi/a$. The phenomenological dispersion relation $q^2 = \epsilon(\omega)\omega^2/c^2$ with the dielectric function $\epsilon(\omega)$, $\omega = E/\hbar$ is a large-wavelength limiting case for our equation. We also obtained another invariant equation for E and q, which has the sense of Ewald's extinction theorem and which for large wavelengths yields the usual macroscopic boundary conditions. The solutions of these equations—obtained analytically and numerically—give the complete set of polariton terms for the number N of monolayers in a pile increasing from $N=1$ to $N \rightarrow \infty$. We traced how two branches of polariton terms with both complex E and q arise and evolve with increasing N. It is shown that when the slab thickness becomes of the order of the wavelength λ strongly radiative polariton states exist which correspond to the cooperative volume of the order of λ^3 and more. After further increasing the slab thickness up to a bulk crystal the radiative width of these states is monotonously decreased to zero. There are no oscillations in this dependence like those obtained in Ref. 9 for polaritons with zero wave vector. A comparison of our results to those of macroscopic electrodynamics is also performed using the new exact phenomenological expression for the radiative damping. This expression takes into account multiple inner reflections of a polariton instead of the approximate one for one inner reflection which was used in previous publications.

II. MODEL HAMILTONIAN AND BASIC EQUATIONS

We will study a molecular crystal slab of a cubic structure consisting of N plane monolayers stacked in the z direction. A monolayer consists of M molecules with ν_e electrons in each. In crystals of the structure of anthracene, tetracene, etc., the widths of the Coulomb exciton bands in the z direction are small compared to $\Gamma^{(2)}$. Therefore, the interaction between such crystalline planes is determined mainly by retarded rather than Coulomb interactions between the molecules localized on crystalline planes, which therefore may be neglected. This approximation works especially well for the exciton states with zero wave vector in the xy plane. These states will be studied in the present work. We also neglect the energy shifts of the outermost monolayers. These shifts were not taken into account in previous publications. Their consideration does not create a problem since it yields only some change in the boundary conditions.[13] One more assumption is made for the sake of simplicity—that the transition dipole moments in all molecules composing the slab have the same orientation in the xy plane.

Thus, neglecting the nonretarded part of the interaction between molecules localized on different planes, the Hamiltonian $\hat{H}$ of the Coulomb excitons interacting with the transverse photons (which are responsible for the retarded interaction) can be written as follows:[2,4]

$$\hat{H} = \hat{H}_{\rm ex} + \hat{H}_{\rm ph} + \hat{H}_{\rm int}^{(1)} + \hat{H}_{\rm int}^{(2)}, \tag{1a}$$

$$\hat{H}_{\rm ex} = \sum_{\mu,n,\mathbf{k}_\parallel} E_\mu(\mathbf{k}_\parallel)\hat{B}^+_{\mu,n}(\mathbf{k}_\parallel)\hat{B}_{\mu,n}(\mathbf{k}_\parallel), \tag{1b}$$

$$\hat{H}_{\rm ph} = \sum_{\mathbf{k},j} \hbar k c \hat{a}^+_{\mathbf{k},j}\hat{a}_{\mathbf{k},j}, \tag{1c}$$

$$\hat{H}_{\rm int}^{(1)} = -\sum_{\mathbf{k},j} \{T^{\mu,n}_{\mathbf{k},j}\hat{a}_{\mathbf{k},j}[\hat{B}_{\mu,n}(-\mathbf{k}_\parallel) - \hat{B}^+_{\mu,n}(\mathbf{k}_\parallel)] + (T^{\mu,n}_{\mathbf{k},j})^*\hat{a}^+_{\mathbf{k},j}[\hat{B}^+_{\mu,n}(-\mathbf{k}_\parallel) - \hat{B}_{\mu,n}(\mathbf{k}_\parallel)]\}, \tag{1d}$$

$$\hat{H}^{(2)}_{\rm int}=\frac{\pi\hbar M\nu_e e^2}{Vmc}$$
$$\times\sum_{n,\mathbf{k}_\parallel}\sum_{k_\perp,j}\sum_{k'_\perp,j'}\frac{(\mathbf{e}_{\mathbf{k}_\parallel,k_\perp,j}\cdot\mathbf{e}_{\mathbf{k}_\parallel,k'_\perp,j'})}{[(k_\parallel^2+k_\perp^2)(k_\parallel^2+(k'_\perp)^2)]^{1/4}}$$
$$\times(2\hat{a}^+_{\mathbf{k}_\parallel,k_\perp,j}\hat{a}_{\mathbf{k}_\parallel,k'_\perp,j'}e^{-i(k_\perp-k'_\perp)na}$$
$$+\hat{a}_{\mathbf{k}_\parallel,k_\perp,j}\hat{a}_{-\mathbf{k}_\parallel,k'_\perp,j'}e^{i(k_\perp+k'_\perp)na}$$
$$+\hat{a}^+_{\mathbf{k}_\parallel,k_\perp,j}\hat{a}^+_{\mathbf{k}_\parallel,k'_\perp,j'}e^{-i(k_\perp+k'_\perp)na}). \tag{1e}$$

Here $E_\mu(\mathbf{k}_\parallel)$ is the energy of a Coulomb exiton in the μth band with the wave vector $\mathbf{k}_\parallel$ in the slab plane, integer $n=1,2,\ldots,N$ enumerates layers in the slab, $\hat{B}^+$ and $\hat{B}$ are boson creation and annihilation operators for excitons, $\hat{a}^+$ and $\hat{a}$ are those for photons, $\mathbf{k}\equiv(\mathbf{k}_\parallel,k_\perp)$ is the photon wave vector with the components in the slab plane and perpendicular to it, and $j=1,2$ enumerates the photon polarizations with the unit polarization vectors $\mathbf{e}_{\mathbf{k},j}$.

The terms $\hat{H}^{(1)}_{\rm int}$, $\hat{H}^{(2)}_{\rm int}$ appear from the parts $(\mathbf{j}\cdot\mathbf{A})$ and $\mathbf{A}^2$ of the interaction of an atomic system with the transverse electromagnetic field with the vector potential

$$\hat{\mathbf{A}}=\sum_{\mathbf{k},j}\left(\frac{2\pi\hbar c}{Vk}\right)^{1/2}\mathbf{e}_{\mathbf{k},j}(\hat{a}_{\mathbf{k},j}e^{i\mathbf{kr}}+\hat{a}^+_{\mathbf{k},j}e^{-i\mathbf{kr}}). \tag{2}$$

The interaction functions $T^{\mu,n}_{\mathbf{k},j}$ have the following form:

$$T^{\mu,n}_{\mathbf{k},j}=-i\left(\frac{2\pi M}{V\hbar ck}\right)^{1/2}E_\mu(\mathbf{k}_\parallel)(\mathbf{P}_\mu\cdot\mathbf{e}_{\mathbf{k},j})\exp(ik_\perp na). \tag{3}$$

Here a is the distance between the monolayers, V is the quantization volume, and $\mathbf{P}_\mu$ is the dipole moment matrix element between the ground and μth excited states of a single molecule.

The polariton spectra may be obtained as poles of the Green function, imaginary parts of which give the decay rates. The poles may be found by diagonalizing the quadratic Hamiltonian (1) with Bogolyubov–Tyablikov transformation[4] to new boson operators $\hat{\xi}^+_\nu,\hat{\xi}_\nu$,

$$\hat{B}_{\mu,n}(\mathbf{k}_\parallel)=\sum_\nu[\hat{\xi}_\nu u^\nu_{\mu,n}(\mathbf{k}_\parallel)+\hat{\xi}^+_\nu v^\nu_{\mu,n}(\mathbf{k}_\parallel)^*], \tag{4a}$$

$$\hat{a}_{\mathbf{k},j}=\sum_\nu[\hat{\xi}_\nu u^\nu_{\mathbf{k},j}+\hat{\xi}^+_\nu(v^\nu_{-\mathbf{k},j})^*]. \tag{4b}$$

Here the functions $u_{\mu,n}(\mathbf{k}_\parallel)$, $v_{\mu,n}(\mathbf{k}_\parallel)$, $u_{\mathbf{k},j}$, $v_{\mathbf{k},j}$, and energy E must satisfy the corresponding system of linear equations. It is easily seen that the Hamiltonian (1) conserves the parallel component of the wave vector (due to the translational symmetry in the x and y directions), so the polariton states may be classified by the value of $\mathbf{k}_\parallel$. For simplicity we will consider only the states with $\mathbf{k}_\parallel=0$. In this case one of the polarizations with $\mathbf{e}_{\mathbf{k},j}\perp\mathbf{P}_\mu$ is canceled. We will denote the other one by j_0 and use the notations $u_{\mu,n}(\mathbf{k}_\parallel=0)\equiv u_{\mu,n}$, $v_{\mu,n}(\mathbf{k}_\parallel=0)\equiv v_{\mu,n}$, $u_{\mathbf{k}_\parallel=0,k_\perp,j_0}\equiv u_{k_\perp}$, $v_{\mathbf{k}_\parallel=0,k_\perp,j_0}\equiv v_{k_\perp}$, $E_\mu(\mathbf{k}_\parallel=0)\equiv E_\mu$, omitting the subscript j_0 everywhere. Then Bogolyubov–Tyablikov equations for the eigenfunctions u, v and the eigenvalue E may be written in the following form:

$$(\hbar c|k_\perp|-E)u_{k_\perp}+\sum_{\mu,n}(T^{\mu,n}_{k_\perp})^*(u_{\mu,n}-v_{\mu,n})$$
$$+\frac{2\pi\hbar M\nu_e e^2}{Vmc}\sum_{n,k'_\perp}\frac{e^{-i(k_\perp-k'_\perp)na}}{\sqrt{|k_\perp||k'_\perp|}}(u_{k'_\perp}+v_{k'_\perp})=0, \tag{5a}$$

$$(\hbar c|k_\perp|+E)v_{k_\perp}+\sum_{\mu,n}(T^{\mu,n}_{k_\perp})^*(u_{\mu,n}-v_{\mu,n})$$
$$+\frac{2\pi\hbar M\nu_e e^2}{Vmc}\sum_{n,k'_\perp}\frac{e^{-i(k_\perp-k'_\perp)na}}{\sqrt{|k_\perp||k'_\perp|}}(u_{k'_\perp}+v_{k'_\perp})=0, \tag{5b}$$

$$(E_\mu-E)u_{\mu,n}+\sum_{k_\perp}T^{\mu,n}_{k_\perp}(u_{k_\perp}+v_{k_\perp})=0, \tag{5c}$$

$$(E_\mu+E)u_{\mu,n}-\sum_{k_\perp}T^{\mu,n}_{k_\perp}(u_{k_\perp}+v_{k_\perp})=0. \tag{5d}$$

We will study polariton states for one isolated exciton band $\mu=0$ assuming other bands to be well separated from it in the energy domain. Then after some calculations shown in detail in the Appendix we obtain the equation for $u_{\mu=0,n}\equiv u_n$ and the complex energy $E=E'-iE''$,

$$(E^2-E_0^2)u_n+i\Gamma^{(2)}E\sum_{n'=1}^{N}\exp\left(i\frac{Ea}{\hbar c}|n-n'|\right)u_{n'}=0,$$
$$\Gamma^{(2)}\equiv\frac{4\pi|P_0|^2}{a^2}\frac{E_0}{\hbar c}. \tag{6}$$

This equation will be the basic one to solve in the following sections. For one monolayer $(N=1)$ its solution is

$$E=\sqrt{E_0^2-\left(\frac{\Gamma^{(2)}}{2}\right)^2}-i\frac{\Gamma^{(2)}}{2}. \tag{7}$$

Here $E''=\Gamma^{(2)}/2$ is the superradiant radiative linewidth of a 2D crystal, which exceeds that of an isolated molecule by a large factor of the order of $(\lambda/a)^2$,

$$\Gamma^{(2)}=\frac{3}{\pi}\left(\frac{\lambda}{2a}\right)^2\Gamma^{(0)},\quad \Gamma^{(0)}=\frac{4}{3}|P_0|^2\left(\frac{E_0}{\hbar c}\right)^3. \tag{8}$$

An equation similar to Eq. (6) was obtained by Philpott[8] for the amplitudes of oscillating classical dipoles.

We will seek the solutions of Eq. (6) in the form

$$u_n=Ae^{iqna}+Be^{-iqna}, \tag{9}$$

where complex $q=q'-iq''$ for large N has the sense of the wave vector of a polariton in the medium. This as well as the complex E should be found from Eq. (6). Further we denote $K\equiv E/\hbar c$ for brevity. Substitution of Eq. (9) into Eq. (6) yields a set of terms with functions $\exp(\pm iqna)$ and $\exp(\pm iKna)$ which should cancel each other independently. The requirement for cancellation of the terms with $\exp(\pm iqna)$ gives the dispersion relation

$$\cos qa=\cos Ka+\Gamma^{(2)}E\,\frac{\sin Ka}{E^2-E_0^2}. \tag{10}$$

Note that the wave vector q appears here in the invariant form under the transformation $q\to q+2\pi m/a$ with an integer m. In the approximation of phenomenological electrodynamics, $qa\ll 1$, $Ka\ll 1$, Eq. (10) is reduced to the ordinary definition of a dielectric function,

$$\epsilon(\omega)=1-\frac{2c\Gamma^{(2)}}{\hbar a}\,\frac{1}{\omega^2-\omega_0^2},\quad \epsilon(\omega)\equiv q^2/K^2,\quad \omega=E/\hbar. \tag{11}$$

System (6) is invariant with respect to the transformation $n\leftrightarrow N-n+1$, so its solutions can be either symmetric or antisymmetric. The requirement for cancellation of the terms $\exp(\pm iKna)$ in Eq. (6) for the symmetric polariton states ($u_n=u_{N-n+1}$) has the form

$$\cos\left(qa\,\frac{N+1}{2}\right)=e^{iKa}\,\cos\left(qa\,\frac{N-1}{2}\right), \tag{12a}$$

and for the antisymmetric states ($u_n=-u_{N-n+1}$) it is

$$\sin\left(qa\,\frac{N+1}{2}\right)=e^{iKa}\,\sin\left(qa\,\frac{N-1}{2}\right). \tag{12b}$$

Equations (12a) and (12b) correspond to the extinction theorem in the classical optics derived long ago by Ewald. An expansion of Eq. (12) in the case when $qa\ll 1$, $Ka\ll 1$, $N\gg 1$ reduces Eq. (12) to the following form:

$$\tan\left(q\,\frac{Na}{2}\right)=-i\,\frac{K}{q}, \tag{13a}$$

$$\tan\left(q\,\frac{Na}{2}\right)=-i\,\frac{q}{K}, \tag{13b}$$

which coincides with the boundary conditions for a thick slab in macroscopic electrodynamics.[7]

On this stage it is interesting to discuss the difference between our approach and Knoester's.[9,10] In Ref. 9 the problem was treated in momentum space,

$$u_k=\sum_{n=1}^{N}\frac{e^{-ikna}}{\sqrt{N}}\,u_n,\quad k=\frac{2\pi m}{Na},\quad m=0,1,\ldots,N-1. \tag{14}$$

In this representation the kernel of Eq. (6) has the off-diagonal (k,k') elements which were neglected in Ref. 9. This means that in Ref. 9 the reconstruction of the eigenstates was not taken into account, supposing that the wave vector k so defined stays to be a good quantum number after the exciton–photon interaction has been ''switched on.'' In Ref. 10 sines were chosen instead of exponents as a basis set but the approach was principally the same.

III. THE POLARITON TERMS: ANALYTICAL RESULTS

The solutions of Eq. (6) for $N=2$, 3, and 4 can be found in the analytical form. These solutions will be used for a comparison with numerical results.

For $N=2$ from Eq. (6) we obtain two equations for the symmetric ($u_1=u_2$) and antisymmetric ($u_1=-u_2$) polariton states with energies $E=E_s,E_a$,

$$E_s^2=E_0^2+i\Gamma^{(2)}E_s=-i\Gamma^{(2)}E_s\,\exp(iE_sa/\hbar c), \tag{15a}$$

$$E_a^2-E_0^2+i\Gamma^{(2)}E_a=i\Gamma^{(2)}E_a\,\exp(iE_aa/\hbar c). \tag{15b}$$

For the arbitrary parameters E_0 and $\Gamma^{(2)}$ these equations cannot be solved analytically. But in typical crystals the values $E_0a/\hbar c$ and $\Gamma^{(2)}a/\hbar c$ are small: $E_0a/\hbar c\ll 1$, $\Gamma^{(2)}a/\hbar c\ll 1$, and $\Gamma^{(2)}\ll E_0$. In this case we may expand the exponents and obtain the approximate solutions

$$E_s=E_0+\frac{\Gamma^{(2)}}{2}\left(\frac{E_0a}{\hbar c}\right)-i\Gamma^{(2)}\left[1-\frac{1}{2}\left(\frac{E_0a}{\hbar c}\right)^2\right], \tag{16a}$$

$$E_a=E_0-\frac{\Gamma^{(2)}}{2}\left(\frac{E_0a}{\hbar c}\right)-i\,\frac{\Gamma^{(2)}}{4}\left(\frac{E_0a}{\hbar c}\right)^2. \tag{16b}$$

It is seen from Eq. (16a) that the symmetric polariton term has the energy $E_s'>E_0$, and its radiative widths $E_s''\approx\Gamma^{(2)}$, which is almost two times greater than that for $N=1$. This term should be considered to be the beginning of the upper radiative polariton branch for larger N. The antisymmetric term (16b) has the energy $E_a'<E_0$ and its radiative width is several orders of magnitude less than $\Gamma^{(2)}$. This term obviously corresponds to the lower nonradiative polariton branch. The wave vectors of these terms q_s,q_a may be found from Eq. (10) (only the main terms of the expansion are shown),

$$q_s'=q_s''=\sqrt{E_0/2\hbar ca}, \tag{17}$$

$$q_a'=\pi/2a,\quad q_a''=E_0/2\hbar c. \tag{18}$$

Solution of the system (6) for $N=3$ yields three equations for the energy E,

$$E_s^2=E_0^2+i\Gamma^{(2)}E_s$$
$$=-i\Gamma^{(2)}E_s\left[\frac{e^{2iE_sa/\hbar c}}{2}\pm\sqrt{\left(\frac{e^{2iE_sa/\hbar c}}{2}\right)^2+2e^{2iE_sa/\hbar c}}\right], \tag{19a}$$

$$E_a^2-E_0^2+i\Gamma^{(2)}E_a=i\Gamma^{(2)}E_ae^{2iE_aa/\hbar c}. \tag{19b}$$

One of the two symmetric polariton terms which corresponds to the plus sign in Eq. (19a) has the energy

$$E_{1s}=E_0+\frac{4\Gamma^{(2)}}{3}\,\frac{E_0a}{\hbar c}-i\,\frac{\Gamma^{(2)}}{2}\left[3-\frac{56}{27}\left(\frac{E_0a}{\hbar c}\right)^2\right]. \tag{20}$$

We see that the radiative width of this term is very close to $3\Gamma^{(2)}/2$, i.e., three times greater than the width for the isolated monolayer. The real part of the energy $E_{1s}'>E_0$ and we conclude that this term belongs to the upper branch. Substitution of this value into Eq. (10) gives the wave vector of this polariton term,

$$q_{1s}'=q_{1s}''=\sqrt{E_0/3\hbar ca}. \tag{21}$$

The second symmetric term with the minus sign in Eq. (19a) has the energy

$$E_{2s}=E_0-\frac{\Gamma^{(2)}}{3}\frac{E_0a}{\hbar c}-i\frac{\Gamma^{(2)}}{27}\left(\frac{\Gamma^{(2)}a}{\hbar c}\right)^2 \tag{22}$$

and corresponds to the lower branch. From Eq. (10) we have for its wave vector

$$\cos q_{2s}a=-\frac{1}{2}+i\frac{E_0a}{6\hbar c}, \tag{23}$$

which gives

$$q'_{2s}=\frac{2\pi}{3a},\quad q''_{2s}=\frac{1}{3\sqrt{3}}\frac{E_0}{\hbar c}. \tag{24}$$

An analysis of Eq. (19b) for the antisymmetric polariton terms shows that it also has two solutions. The first one has the energy

$$E_{1a}=E_0-\Gamma^{(2)}\frac{E_0a}{\hbar c}-i\Gamma^{(2)}\left(\frac{\Gamma^{(2)}a}{\hbar c}\right)^2 \tag{25}$$

and the wave vector

$$q'_{1a}=\frac{\pi}{3a},\quad q''_{1a}=\frac{1}{\sqrt{3}}\frac{E_0}{\hbar c}. \tag{26}$$

This term belongs to the lower branch.

The second solution of Eq. (19b) corresponds to the upper radiative branch and its energy is very large, $E\gg E_0$, $Ea/\hbar c\sim 1$. In this case we cannot use the expansion as it was done before. First of all we explicitly write down the real and imaginary parts of the equation,

$$E'^2-E''^2-E_0^2+\Gamma^{(2)}E''=\Gamma^{(2)}e^{2E''a/\hbar c}[E''\cos(2E'a/\hbar c)-E'\sin(2E'a/\hbar c)], \tag{27a}$$

$$-2E'E''+\Gamma^{(2)}E'=\Gamma^{(2)}e^{2E''a/\hbar c}[E'\cos(2E'a/\hbar c)+E''\sin(2E'a/\hbar c)]. \tag{27b}$$

Assuming E_0, $\Gamma^{(2)}\ll E'$, and $\Gamma^{(2)}\ll E''$, we omit E_0 and $\Gamma^{(2)}$ in the left-hand side of the equations. For brevity we denote $E'a/\hbar c\equiv x$, $E''a/\hbar c\equiv y$, and $\Gamma^{(2)}a/\hbar c\equiv\gamma$. Replacing the equations with their linear combinations, we obtain

$$y=-2\gamma e^{2y}\cos 2x, \tag{28a}$$

$$x=-2\gamma e^{2y}\sin 2x. \tag{28b}$$

We assume these equations to have a solution with $x\approx\pi/2$. If we use the notation $x=\pi/2+\tilde{x}$, $\tilde{x}\ll 1$, the equations are reduced to

$$y=2\gamma e^{2y}\cos 2\tilde{x}\approx 2\gamma e^{2y}, \tag{29a}$$

$$\frac{\pi}{2}-\tilde{x}=2\gamma e^{2y}\tan 2\tilde{x}. \tag{29b}$$

Since $\gamma\ll 1$ the first equation has the solution

$$2y=-\ln 2\gamma+\ln y\sim-\ln\gamma\gg 1. \tag{30}$$

The second equation is satisfied when

$$\tilde{x}\approx\frac{\pi}{4y}\ll 1. \tag{31}$$

Returning to the dimensional quantities, we have

$$E'_{2a}=\frac{\pi}{2}\frac{\hbar c}{a}\left(1+\frac{\hbar c}{2E''_{2a}a}\right), \tag{32a}$$

$$E''_{2a}\sim\frac{\hbar c}{2a}\ln\left(\frac{\hbar c}{\Gamma^{(2)}a}\right). \tag{32b}$$

The wave vector of this term may again be obtained from Eq. (10). It shows that this term is situated very close to the light axis

$$q\approx E/\hbar c. \tag{33}$$

The logarithmic dependence of E'' on $\Gamma^{(2)}$ is also obtained from the phenomenological approach [see below Eq. (52)].

We now pay more attention to the physical peculiarities of this term. First, we see that $E'_{2a}\gg E_0$ though for all previous terms we had $E'\approx E_0$. For anthracene crystal, $E_0a/\hbar c\approx 10^{-2}$, $\Gamma^{(2)}a/\hbar c\approx 2\cdot 10^{-6}$, and the corresponding $E'_{2a}\sim 10^2$ eV. But our results were obtained under the assumption of one isolated exciton band and for this energy range higher excitation levels must be taken into account. The second feature is that the width of this term is several times greater than the energy itself (for anthracene parameters $E''_{2a}\sim 5E'_{2a}$). This means that we are beyond the concept of a quasiparticle as an elementary excitation. So we can conclude that this solution has no physical meaning, but mathematically it is essential for the completeness of the set of solutions of system (6). We shall see below that for larger $N=4,5,\ldots$ some more analogous terms will appear, their widths being less than E''_{2a} and monotonously decreasing to zero as the slab thickness increases to the bulk crystal.

Thus we have found two terms for $N=2$ and four terms for $N=3$. We shall see later that this is a general rule: For N monolayers the total number of terms in the first Brillouin zone is $2(N-1)$, of which $N-1$ belong to the radiative branch and $N-1$ to the nonradiative one. In each branch symmetric and antisymmetric terms are alternating, starting from the symmetric one with the smallest q' in the upper branch and the antisymmetric one in the lower branch. The distance between neighboring terms in each branch is approximately $\delta q'\approx\pi/Na$. We will designate terms by an integer number (which is the number of the term in the corresponding branch with q' growing: $q'_1<q'_2<q'_3<\cdots$) and a letter ''s'' or ''a'' showing the symmetry of this term. According to the rule mentioned above, the upper branch gives the sequence $1s,2a,3s,4a,\ldots$ and the lower branch—$1a,2s,3a,4s,\ldots$. Note that such marks unambiguously determine the branch to which the term belongs.

For the slab of four monolayers we have two equations for the symmetric states and two for the antisymmetric states,

$$E_s^2-E_0^2+i\Gamma^{(2)}E_s=i\Gamma^{(2)}E_s\left[\frac{Z_s+Z_s^3}{2}\pm\sqrt{\left(\frac{Z_s-Z_s^3}{2}\right)^2+(Z_s+Z_s^2)^2}\right], \tag{34a}$$

$$E_a^2-E_0^2+i\Gamma^{(2)}E_a=i\Gamma^{(2)}E_a\left[\frac{Z_a+Z_a^3}{2}\pm\sqrt{\left(\frac{Z_a-Z_a^3}{2}\right)^2+(Z_a+Z_a^2)^2}\right], \tag{34b}$$

$Z\equiv\exp(iEa/\hbar c)$.

For the $1s$ term $E_{1s}\approx E_0$ and the usual expansion gives us

$$E_{1s}=E_0+\frac{5\Gamma^{(2)}}{2}\frac{E_0a}{\hbar c}-i\frac{\Gamma^{(2)}}{2}\left[4-\frac{21}{4}\left(\frac{E_0a}{\hbar c}\right)^2\right], \tag{35}$$

$$q'_{1s}=q''_{1s}=\sqrt{\frac{E_0}{4\hbar ca}}. \tag{36}$$

It is seen that for small N the radiative width of the $1s$ term is proportional to N: $E''_{1s}(N)\approx N\Gamma^{(2)}/2$. This dependence is in agreement with Ref. 9 and is confirmed by numerical results discussed further.

Using the procedure analogous to that used for the $2a$ term for $N=3$ one can find two solutions with large energies at $q'_{2a}a\approx\pi/3$ and $q'_{3s}a\approx 2\pi/3$. These solutions lie very close to the light axis, $q\approx E/\hbar c$,

$$E_{2a}=\frac{\pi}{3}\frac{\hbar c}{a}-i\frac{\hbar c}{3a}\ln\left(\frac{\hbar c}{\Gamma^{(2)}a}\right), \tag{37a}$$

$$E_{3s}=\frac{2\pi}{3}\frac{\hbar c}{a}-i\frac{\hbar c}{3a}\ln\left(\frac{\hbar c}{\Gamma^{(2)}a}\right). \tag{37b}$$

The widths of the $2a$ and $3s$ terms are close and both are less than the width of the $2a$ term in the previous case with $N=3$. It will be seen that the widths of terms (except the $1s$ term) in the upper branch monotonously decrease to zero as N increases so that $E''_{2a}(N=3)$ is the upper limit for E''. The inverse proportionality of E'' for the upper terms to N is also in agreement with the phenomenologic formula (52).

The terms $1a$,$2s$,$3a$ in the lower branch $E'<\hbar cq'$ have the following energies near E_0:

$$E_{1a}=E_0-\frac{\Gamma^{(2)}}{2}\frac{E_0a}{\hbar c}(2+\sqrt{2})-i\frac{\Gamma^{(2)}}{2}\left(\frac{E_0a}{\hbar c}\right)^2\times\left(\frac{5}{2}+\frac{7}{2\sqrt{2}}\right), \tag{38}$$

$$E_{2s}=E_0-\frac{\Gamma^{(2)}}{2}\frac{E_0a}{\hbar c}-i\frac{\Gamma^{(2)}}{2}\left(\frac{E_0a}{\hbar c}\right)^2\frac{1}{4}, \tag{39}$$

$$E_{3a}=E_0-\frac{\Gamma^{(2)}}{2}\frac{E_0a}{\hbar c}(2-\sqrt{2})-i\frac{\Gamma^{(2)}}{2}\left(\frac{E_0a}{\hbar c}\right)^2\times\left(\frac{5}{2}-\frac{7}{2\sqrt{2}}\right). \tag{40}$$

The wave vectors of these terms may be easily obtained as described above.

It is also possible to study analytically the case of large N: $N\gg(E_0a/\hbar c)^{-1}$. We will focus on the characteristics of the $1s$ term as a function of N. First we substitute the value of E from Eq. (12a) into Eq. (11). The latter takes the form

$$E_0^2+(\hbar cq)^2\tan^2\left(\frac{Nqa}{2}\right)+2(\Gamma^{(2)}\hbar c/a)\sin^2\left(\frac{Nqa}{2}\right)=0. \tag{41}$$

We seek a solution near π/Na: $q=\pi/Na-2\zeta/Na$, $\zeta\ll 1$. Approximating $\cot\zeta=1/\zeta$, we have

$$E_0^2+2(\Gamma^{(2)}\hbar c/a)+\left(\frac{\pi\hbar c}{Na}\right)^2\frac{1}{\zeta^2}=0. \tag{42}$$

So we conclude that

$$\zeta=\frac{i\pi}{N}\frac{c}{\Omega_\parallel a}\sim\frac{1}{N}, \tag{43}$$

$$q_{1s}=\frac{\pi}{Na}-i\frac{2\pi}{N^2a}\frac{c}{\Omega_\parallel a}, \tag{44}$$

$$(\hbar\Omega_\parallel)^2\equiv E_0^2+2\Gamma^{(2)}\hbar c/a, \tag{45}$$

where $\Omega_\parallel$ is the frequency of the longitudinal waves with $\varepsilon(\Omega_\parallel)=0$.

Now we seek the energy of this term: $E=\hbar\Omega_\parallel+\epsilon$, $\epsilon\ll\hbar\Omega_\parallel$. From Eq. (11) we obtain

$$(\hbar cq)^2=E^2\frac{E^2-(\hbar\Omega_\parallel)^2}{E^2-E_0^2}=\frac{(\hbar\Omega_\parallel)^2+2\hbar\Omega_\parallel\epsilon+\epsilon^2}{2\Gamma^{(2)}/\hbar c+2\hbar\Omega_\parallel\epsilon+\epsilon^2}(2\hbar\Omega_\parallel+\epsilon)\epsilon. \tag{46}$$

Since we are interested only in the main terms of the expansion of ϵ in the orders of $1/N$, we may write

$$\epsilon=\frac{\Gamma^{(2)}c^3}{\Omega_\parallel^3a^3}(qa)^2=\frac{\Gamma^{(2)}c^3}{\Omega_\parallel^3a^3}\frac{\pi^2}{N^2}-i\frac{\Gamma^{(2)}c^4}{\Omega_\parallel^4a^4}\frac{4\pi^2}{N^3}. \tag{47}$$

Thus we may conclude that the radiative width of the $1s$ term, i.e., the term in the upper branch with the lowest energy and the smallest value of q, at large N is proportional to $1/N^3$. There are no oscillations like those obtained in Refs. 9 and 10 for the states which are not eigenstates. Nevertheless in Ref. 10 the correct behavior of the envelope function was found ($1/N^3$ instead of $1/N$ in Ref. 9) due to the better choice of zeroth approximation states.

We will also compare our microscopic results obtained from Eqs. (10) and (12) to the radiative widths obtained from

the phenomenological electrodynamics in the following way. Let us consider a wave package traveling inside the slab with the phenomenological group velocity

$$v_{\mathrm{gr}}=\frac{d\omega}{dq} \tag{48}$$

and reflecting from its edges. The time between two successive reflections is $\tau=Na/v_{\mathrm{gr}}$. The Fresnel reflection coefficient at the boundary ''crystal/vacuum'' is

$$R=\left|\frac{\sqrt{\varepsilon}-1}{\sqrt{\varepsilon}+1}\right|^2, \tag{49}$$

where $\varepsilon=\varepsilon(\omega)$ is the dielectric function (11), then the probability for the package to remain inside the slab after the time t having made $\nu=t/\tau$ successive reflections is

$$P(t)=R^{\nu}=R^{t/\tau}=\exp\left(\frac{t}{\tau}\ln R\right)=\exp\left(\frac{t}{Na/v_{\mathrm{gr}}}\ln R\right). \tag{50}$$

On the other hand, by definition

$$P(t)=e^{-2E''_{\mathrm{ph}}t/\hbar}. \tag{51}$$

The coefficient 2 stands here because E''_{ph} is the decay rate for the amplitude. So we conclude that

$$E''_{\mathrm{ph}}=\frac{\hbar v_{\mathrm{gr}}}{2Na}\ln\frac{1}{R}. \tag{52}$$

In the case $1-R\ll 1$ the logarithm may be expanded and we obtain the expression used in Refs. 5 and 9,

$$E''_{\mathrm{ph}}=\frac{\hbar v_{\mathrm{gr}}}{2Na}(1-R). \tag{53}$$

We will compare the microscopic results to Eq. (52). It may be shown that the latter gives much better agreement than Eq. (53). It may be seen particularly well at large ω when $\varepsilon(\omega)\to 1$, $R\to 0$. As $\varepsilon(\omega)-1\propto\Gamma^{(2)}$, Eq. (52) is in agreement with the result obtained by the solution of Eqs. (10) and (12) for small $N=3,4$ where we had $E''\propto -N^{-1}\ln(\Gamma^{(2)}a/\hbar c)$.

IV. THE POLARITON TERMS: NUMERICAL RESULTS

Equations (10) and (12) were solved numerically by means of the following inverted scheme. We have two real-valued parameters E_0 and $\Gamma^{(2)}$ that are fixed for some real crystal. We also have four unknown real-valued quantities q', q'', E', and E''. The main idea of the method is that Eqs. (10) and (12) define two explicit functions $E_0(q',q'')$ and $\Gamma^{(2)}(q',q'')$ as described below. Let us set some values q' and q''. The complex dependence $E=E(q)$ is easily obtained from Eq. (12a) for the symmetric states and from Eq. (12b) for the antisymmetric states,

$$K(q)\equiv\frac{E(q)}{\hbar c}=\frac{1}{ia}\ln\left[\cos\left(qa\,\frac{N+1}{2}\right)\Big/\cos\left(qa\,\frac{N-1}{2}\right)\right], \tag{54a}$$

$$K(q)\equiv\frac{E(q)}{\hbar c}=\frac{1}{ia}\ln\left[\sin\left(qa\,\frac{N+1}{2}\right)\Big/\sin\left(qa\,\frac{N-1}{2}\right)\right]. \tag{54b}$$

From these equations we have the quantities $E'=E'(q',q'')$ and $E''=E''(q',q'')$ for the previously set q' and q''. Equation (10) may be written identically in the form linear with respect to the quantities E_0^2 and $\Gamma^{(2)}$,

$$E_0^2[\cos(qa)-\cos(Ka)]+\Gamma^{(2)}E\,\sin(Ka)=E^2[\cos(qa)-\cos(Ka)]. \tag{55}$$

Substitution of the quantities q', q'', E', and E'' known from above into the complex equation (55) yields two linear equations for the real E_0^2 and $\Gamma^{(2)}$ which can be solved directly using Kramer's rule,

$$E_0=\sqrt{\frac{\Phi'_3\Phi''_2-\Phi''_3\Phi'_2}{\Phi'_1\Phi''_2-\Phi''_1\Phi'_2}},\quad \Gamma^{(2)}=\frac{\Phi'_1\Phi''_3-\Phi''_1\Phi'_3}{\Phi'_1\Phi''_2-\Phi''_1\Phi'_2}, \tag{56}$$

where real and imaginary parts of the complex functions $\Phi_j=\Phi'_j-i\Phi''_j$ are obtained from

$$\Phi_1(q,E)=\cos qa-\cos Ka,\quad \Phi_2(q,E)=E\,\sin Ka,$$
$$\Phi_3(q,E)=E^2\Phi_1(q,E). \tag{57}$$

With this scheme the whole problem of the analytical solution for Eqs. (10) and (12) is completed because the direct connection between all quantities E_0, $\Gamma^{(2)}$, q', q'', E'', and E'' is found. Each pair (q',q'') that yields a given E_0 and $\Gamma^{(2)}$ in this way corresponds to the polariton term with the wave vector $q=q'-iq''$ and energy $E=E'-iE''$ in the crystal with the parameters E_0 and $\Gamma^{(2)}$. Then the simple computational task is to choose in the 2D region $0<q'<\pi/a$, $0<q''$ points (q',q'') that give us by this inverted procedure the fixed E_0 and $\Gamma^{(2)}$.

In real molecular crystals studied experimentally the intersection of the photon and exciton branches in the plane (q,E) occurs at the value of the wave vector $q_0=E_0/\hbar c\sim(10^{-3}/10^{-2})\pi/a$, which is much less than the Brillouin zone boundary π/a. For the singlet exciton in the anthracene crystal $q_0=4\times 10^{-3}\pi/a$. For real crystals we are interested in spectra at $N\sim 1/q_0a\sim 10^2$, which is far from the beginning of the row $N=1,2,3,...,100,...$. So the real anthracene parameters are inconvenient for demonstration of the full set of polariton terms in the first Brillouin zone. For this reason as the first step before the calculation of polariton terms for anthracene we have studied the polariton spectra of a crystal slab with the parameters $E_0a/\hbar c=0.5$ and $\Gamma^{(2)}a/\hbar c=0.1$

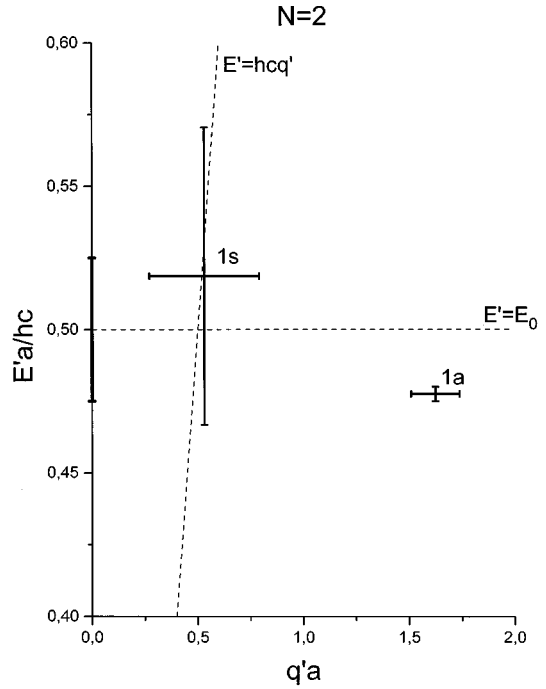

FIG. 1. The polariton terms in the phase plane (q',E') for the crystal slab with two monolayers. The center of a cross is in the point $(q'a,E'a/\hbar c)$ corresponding to the real parts of the wave vector and the energy of the polariton, the sizes of the horizontal and vertical ''error bars'' are equal to $q''a$ and $E''a/\hbar c$. The dashed lines represent exciton and photon unperturbed dispersion laws $[E(q)=E_0,\ E(q)=\hbar cq]$. $N=2$, $E_0a/\hbar c=0.5$, $\Gamma^{(2)}a/\hbar c=0.1$.

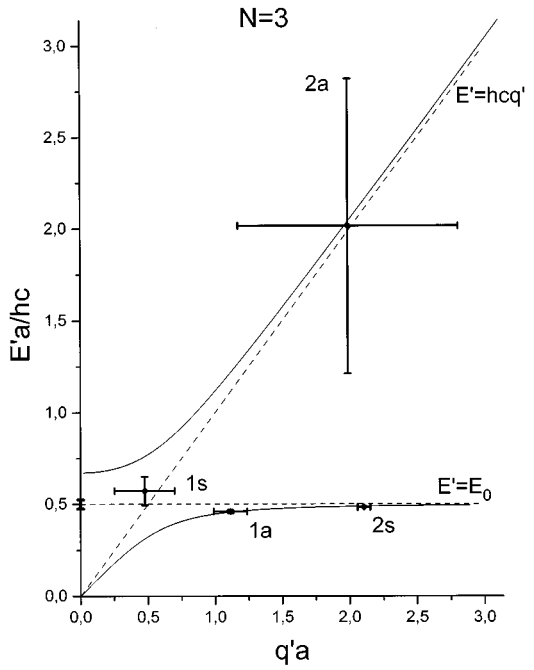

FIG. 2. The polariton terms for the slab with three monolayers. The solid lines are polariton branches of the bulk crystal. $N=3$, $E_0a/\hbar c=0.5$, $\Gamma^{(2)}a/\hbar c=0.1$.

which correspond to a small value $\lambda/a=12$. These parameters allow us to trace in detail the polariton terms generated in the Brillouin zone as the number of monolayers increases starting from $N=1$. The qualitative picture of the forming of the polariton spectrum will be seen at these values of E_0 and $\Gamma^{(2)}$. By the way, the same problem of retarded interaction between multipoles is urgent for x-ray ($\lambda\sim a$) and γ-quantum regions $\lambda\ll a$ (see, e.g., Ref. 14). Then the results for slabs with high energy E_0 and strong interaction $\Gamma^{(2)}$ may be useful in these fields.

The polariton spectra for the slab thicknesses $N=2,3,4,12$, and 33 are shown in Figs. 1–5 on the plane (q',E'). The full Brillouin zone $0\leqslant q'\leqslant\pi/a$ is shown. The polariton terms are shown by crosses. The center of a cross is placed at the point (q',E') which is the solution of Eqs. (10), (12a) or (10), (12b). ''Error bars'' show the imaginary parts q'' and E'' accordingly. Numeration of the terms for the upper radiative polariton branch in the positive direction of q' yields the sequence $1s,2a,3s,4a,\ldots$ of the symmetric (s) and antisymmetric (a) terms. For the lower nonradiative branch this sequence is $1a,2s,3a,4s,\ldots$. The energy E_0 and the width $\Gamma^{(2)}/2$ at $N=1$ are shown on the $q'=0$ axis by a bold bar of length $\Gamma^{(2)}/2$ centered at $E'=E_0$. The dispersion curve $q'=(E'/\hbar c)\sqrt{\epsilon(\omega')}$ is shown in Figs. 4 and 5 as the thick center line between two adjacent thin lines. The distance between the thin lines along the E' axis is equal to $E''_{\rm ph}$ calculated from Eq. (52). Then the fit of a polariton cross between the thin lines is a measure of coincidence between the macroscopic and microscopic theories. At $q'=0$ the dispersion curve for the upper branch gives the energy of the longitudinal waves with $\epsilon=0$.

For $N=2$ there are two polariton terms (Fig. 1). One of them is placed in the radiative region $E'>\hbar cq'$ and the

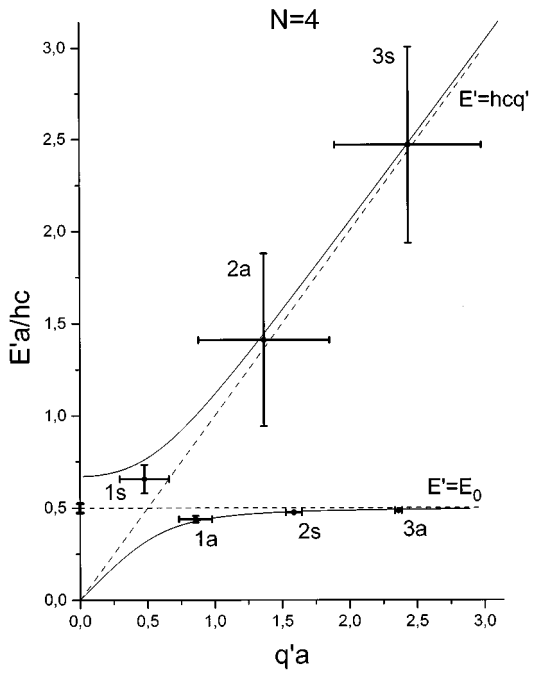

FIG. 3. The polariton terms for the slab with four monolayers. $N=4$, $E_0a/\hbar c=0.5$, $\Gamma^{(2)}a/\hbar c=0.1$.

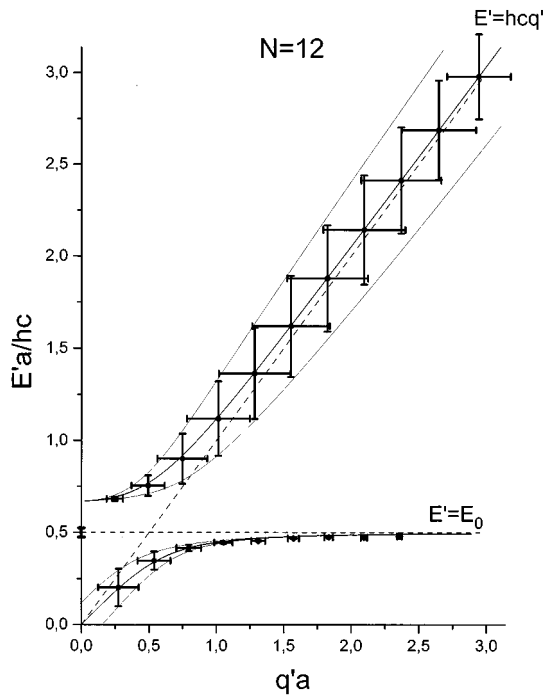

FIG. 4. The polariton terms for the slab with thickness equal to the light wavelength. Some terms in the lower branch at the end of the first Brillouin zone are omitted since they do not contain any new information. The vertical distance between the thin solid lines is equal to the $E''a/\hbar c$ obtained from Eq. (52). $N=12$, $E_0a/\hbar c=0.5$, $\Gamma^{(2)}a/\hbar c=0.1$.

other in the nonradiative region $E'<\hbar cq'$. The first term has the radiative width $E''=\Gamma^{(2)}$ which coincides with Eq. (15a) and the width of the second term is much smaller. This picture is the starting point for both polariton branches.

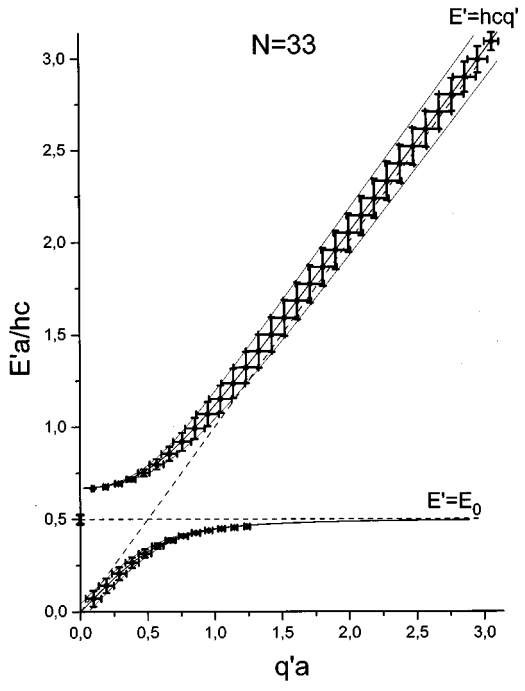

FIG. 5. The polariton terms for the slab with thickness exceeding the light wavelength. $N=33$, $E_0a/\hbar c=0.5$, $\Gamma^{(2)}a/\hbar c=0.1$.

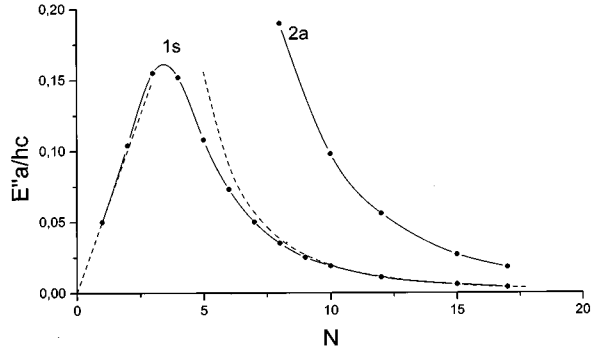

FIG. 6. The dependence of the radiative width on the number of monolayers in the slab for $1s$ and $2a$ terms in the upper radiative polariton branch. The dashed lines show the asymptotes $E''=N\Gamma^{(2)}/2$ for small N and $E''\propto 1/N^3$ for large N [Eq. (47)]. $E_0a/\hbar c=0.5$, $\Gamma^{(2)}a/\hbar c=0.1$.

There are four polariton terms for $N=3$ (Fig. 2) with two terms in the radiative region and two in the nonradiative region. The radiative width E'' of the upper terms is growing with the increasing q' and for the lower terms the situation is the opposite. The uncertainty in wave vector q'' reveals the same behavior. Note that the first $1s$ term in the radiative region has the width $E''\approx 3\Gamma^{(2)}/2$. Also we see the term in the upper branch with $E''\sim E'$, $E'\gg E_0$. Its width is in agreement with the analytical result (32b).

Figures 3–5 together with Figs. 1 and 2 show that with increasing N the number of polariton terms increases as $2(N-1)$ with one-half in the radiative branch and the other half in the nonradiative branch. The positions of the terms on the q' axis are approximately $q'_m a \approx \pi m/N$, $m=1,2,\ldots$. For each N the width of the polariton terms in the radiative region increases with increasing q' and near the end of the Brillouin zone there is a slight decrease. E'' in the nonradiative region decreases monotonously with q'. Comparison of the spectra for different N shows that the radiative width E'' decreases with increasing N and tends to zero for the bulk crystal as it was foreseen. Only the width of the first $1s$ term in the radiative region has nonmonotonous dependence on N. This dependence $E''_{1s}(N)$ is shown in Fig. 6 (the curve labeled $1s$) along with $E''_{2a}(N)$. For small N, $E''_{1s}\approx N\Gamma^{(2)}/2$. Then it reaches a maximum at $N=4=\lambda/3a=N_{\rm cr}$, $E''_{\max}=0.16\approx(\lambda/4a)(\Gamma^{(2)}/2)$ and monotonously decreases to zero for $N>N_{\rm cr}$, in agreement with the analytical estimation (47). The dashed lines show the asymptotical behavior of $E''(N)$ at small $N\gg\lambda/a$, $E''=N\Gamma^{(2)}/2$ and large $N\gg\lambda/a$, $E''=(4\pi^2\Gamma^{(2)}c^3/\Omega_\parallel^4 a^4)N^{-3}$ [Eq. (47)]. We see that for $N>\lambda/a$ the agreement is very good.

Calculations were also performed for the real anthracene crystal. The values of the parameters are $E_0a/\hbar c=10^{-2}$, $\Gamma^{(2)}a/\hbar c=2\times10^{-6}$. In Fig. 7, the $1s$ term for several values of $N=4,50,100,150$ is plotted. Other terms, i.e., $2a,3s,4a,\ldots$, in the upper branch and $1a,2s,3a$, etc., in the lower branch are not shown because they are far in the center of the Brillouin zone. The small value of $\Gamma^{(2)}$ is the reason for the small splitting between the longitudinal frequency $\hbar\Omega_\parallel$ and E_0.

The main features of the polariton spectra for small N compared to λ/a coincide with those in Figs. 1–4. For

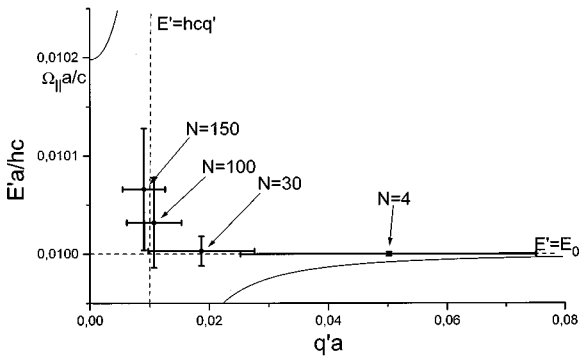

FIG. 7. The polariton term $1s$ in the phase plane (q',E') for the anthracene slab with $N=4$, 30, 50, and 100 monolayers. The rest of the terms $2a$,$3s$ in the upper radiative polariton branch are in an unphysical energy range for one exciton band approximation and they are not shown. The polariton terms $1a$, $2s$, and $3a$ in the lower branch are in the region of wave vectors $qa\sim\pi/N$ and they are far beyond the right edge of this plot. $E_0a/\hbar c=0.01$, $\Gamma^{(2)}a/\hbar c=2.0\times10^{-6}$.

$N\sim\lambda/a$ the amount of polariton terms near the intersection of the exciton and photon branches is large enough for the demonstration on a plot. Figure 8 shows the polariton spectrum at $N=500$. Figure 9 for $N=1000$ and $N=2000$ shows the improvement in coincidence with the phenomenological theory with the growth of N.

Figure 10(a) shows a dependence of E'' on N that is analogous to that in Fig. 6. The thick curves labeled ''$1s$'' and ''$2a$'' represent the dependencies obtained numerically for $1s$ and $2a$ terms. The maximum $E''_{1s\max}=1.5\times10^{-4}=(\lambda/4a)(\Gamma^{(2)}/2)$ is at $N_{\rm cr}=250\sim\lambda/3a$. Note that it is the same as for $E_0a/\hbar c=0.5$, $\Gamma^{(2)}a/\hbar c=0.1$. The dashed lines

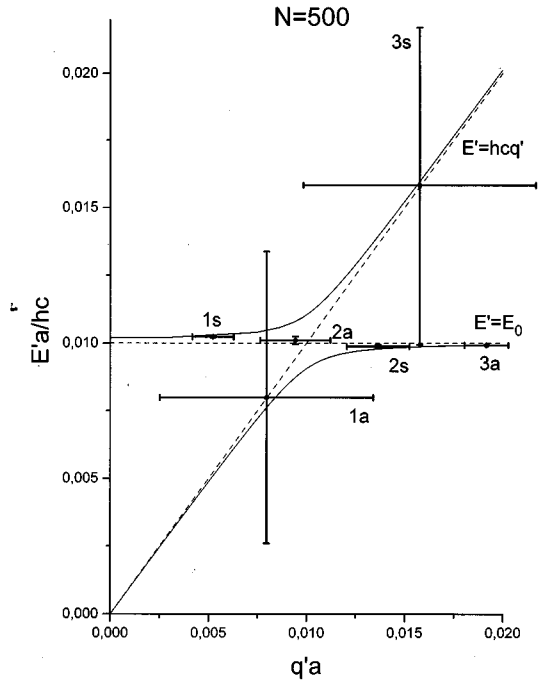

FIG. 8. The polariton terms for the anthracene slab with thickness of the order of the light wavelength. $N=500$, $E_0a/\hbar c=0.01$, $\Gamma^{(2)}a/\hbar c=2.0\times10^{-6}$.

show the analytical dependencies analogous to those in Fig. 6. The thin line shows the dependence obtained in Ref. 9 which coincides with our results for $N<N_{\rm cr}$. For $N>N_{\rm cr}$ the agreement between the numerical results and those from Eq. (47) is not satisfactory, so the case of large N is plotted separately in Fig. 10(b). It is clearly seen in the logarithmic scale with the law $1/N^3$ represented by a straight line that the agreement improves as $N\to\infty$.

V. CONCLUSIONS

We have traced two branches of polariton terms at $k_{\|}=0$ with increasing N. For a finite N we obtained a set of discrete terms. These terms may be classified by the complex wave vector $q=q'-iq''$ (where the imaginary part shows the uncertainty) and the complex energy $E=E'-iE''$ (where the imaginary part $-E''$ gives the decay rate and is always negative). At small N these terms can be seen as resonant peaks in the reflection of the sample or holes in transmission (at normal incidence). Even for small N these terms lie close to the polariton curve of a bulk crystal in the (q,E) plane. The number of terms in the first Brillouin zone is proportional to N, and as N grows the terms become more dense, quasicontinous polariton branches appear and the imaginary parts of their q and E tend to zero, which is the continuous transition to the case of a bulk crystal.

Special attention was paid to the behavior of the decay rates of the polariton terms at small q near the intersection of the exciton and photon axes. We found that the lowest term in the upper branch has the radiative width $E''\approx N\Gamma^{(2)}/2$ at small N, at $N\sim\lambda/a$ it reaches its maximum and after further increasing the slab thickness up to a bulk crystal the radiative width of all states is monotonously decreased to zero as $1/N^3$, exposing no oscillations found in Refs. 9 and 10.

ACKNOWLEDGMENTS

The authors are thankful for partial supports which were received through Grant 1-044, Physics of Solid State Nanostructures, Russian Ministry of Sciences and Grant 96-0334049 of Russian Foundation of Basic Research.

APPENDIX

Here we derive Eq. (6). First, we eliminate $v_{\mu,n}$ and $v_{k_\perp}$,

$$v_{\mu,n}=\frac{E-E_\mu}{E+E_\mu}\,u_{\mu,n},\quad v_{k_\perp}=-\frac{E-\hbar c|k_\perp|}{E+\hbar c|k_\perp|}\,u_{k_\perp}. \tag{A1}$$

On substituting these values into Eqs. (5a) and (5c) the system is reduced to

$$(\hbar c|k_\perp|-E)u_{k_\perp}+\sum_{\mu,n}(T^{\mu,n}_{k_\perp})^*\,\frac{2E_\mu}{E+E_\mu}\,u_{\mu,n}$$

$$+\frac{2\pi\hbar M\nu_e e^2}{Vmc}\sum_{n,k'_\perp}\frac{e^{-i(k_\perp-k'_\perp)na}}{\sqrt{|k_\perp||k'_\perp|}}\,\frac{2\hbar c|k'_\perp|}{E+\hbar c|k'_\perp|}\,u_{k'_\perp}=0, \tag{A2a}$$

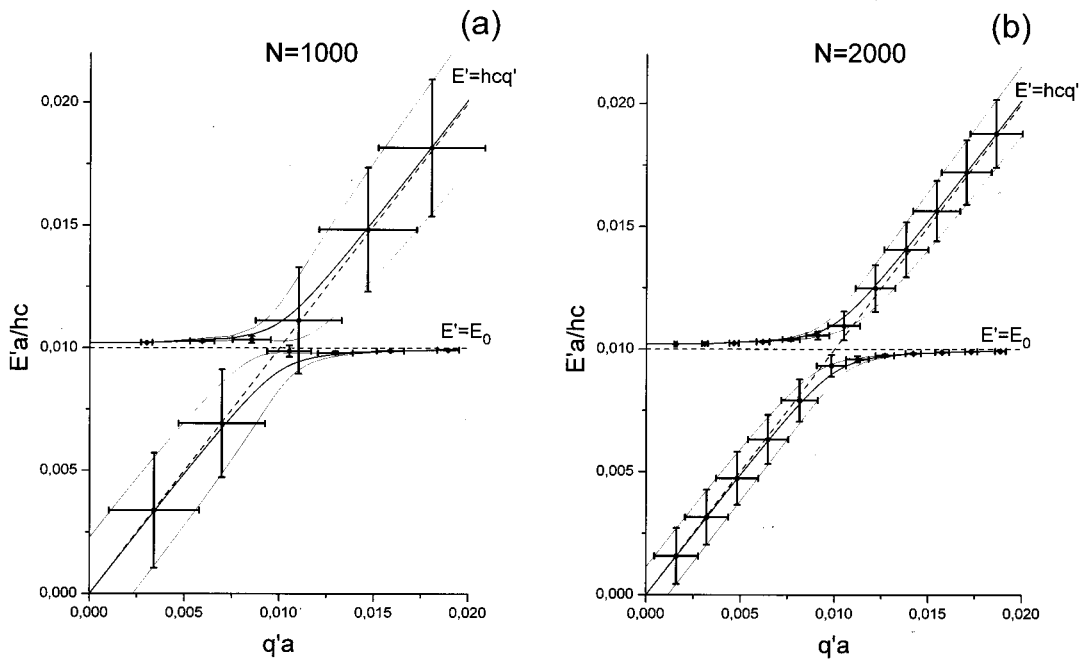

FIG. 9. The polariton terms for the anthracene slabs with thicknesses exceeding the light wavelength—transition to the bulk crystal and convergence of the microscopic and phenomenological results. (a) $N=1000$, $E_0a/\hbar c=0.01$, $\Gamma^{(2)}a/\hbar c=2.0\times10^{-6}$; (b) $N=2000$, $E_0a/\hbar c=0.01$, $\Gamma^{(2)}a/\hbar c=2.0\times10^{-6}$.

$$(E_\mu - E)u_{\mu,n} + \sum_{k_\perp} T^{\mu,n}_{k_\perp} \frac{2\hbar c|k_\perp|}{E+\hbar c|k_\perp|}\, u_{k_\perp} = 0. \tag{A2b}$$

Substitution of $u_{\mu,n}$ from Eq. (A2a) to Eq. (A2b) yields the equation for $u_{k_\perp}$ (here we use the explicit expression for $T^{\mu,n}_{k_\perp}$),

$$(\hbar c|k_\perp| - E)u_{k_\perp} + \frac{2\pi M}{V\hbar c} \times \sum_{n,k'_\perp} \frac{e^{-i(k_\perp - k'_\perp)na}}{\sqrt{|k_\perp||k'_\perp|}} \left[\sum_\mu |\mathbf{P}_\mu|^2 \frac{2E_\mu^3}{E^2 - E_\mu^2} + \frac{\nu_e e^2\hbar^2}{m} \right] \times \frac{2\hbar c|k'_\perp|}{E+\hbar c|k'_\perp|}\, u_{k'_\perp} = 0. \tag{A3}$$

The expression in the square brackets may be rewritten identically as

$$\sum_\mu |\mathbf{P}_\mu|^2 \frac{2E_\mu^3}{E^2 - E_\mu^2} + \frac{\nu_e e^2\hbar^2}{m} \equiv \sum_\mu |\mathbf{P}_\mu|^2 \frac{2E_\mu E^2}{E^2 - E_\mu^2} + \left(\frac{\nu_e e^2\hbar^2}{m} - 2\sum_\mu |\mathbf{P}_\mu|^2 E_\mu \right). \tag{A4}$$

The summation rule[4]

$$2\sum_\mu |\mathbf{P}_\mu|^2 E_\mu \equiv \frac{\nu_e e^2\hbar^2}{m} \tag{A5}$$

eliminates the last term in Eq. (A4). Then new interaction functions may be introduced instead of $T^{\mu,n}_{k_\perp}$,

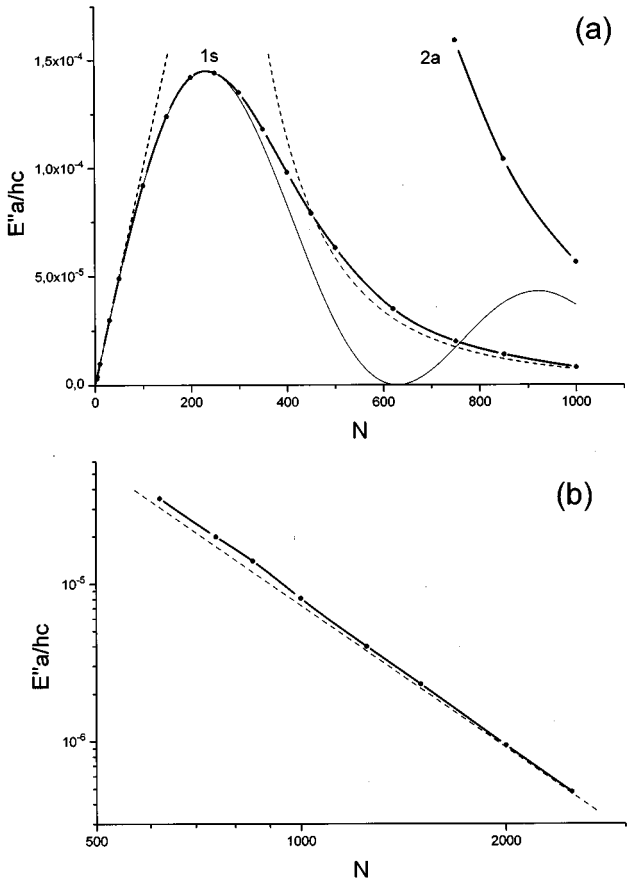

FIG. 10. (a) The dependence of the radiative width on the number of monolayers in the anthracene slab for $1s$ and $2a$ terms in the upper radiative polariton branch, compared to the result of Ref. 9. (b) Demonstration of coincidence of the numerical results and the asymptotic law $E'' \propto 1/N^3$ for large N [Eq. (47)] in logarithmic scale. $E_0a/\hbar c=0.01$, $\Gamma^{(2)}a/\hbar c=2.0\times10^{-6}$.

$$t_{k_\perp}^{\mu,n}=\frac{E}{E_\mu}\,T_{k_\perp}^{\mu,n}. \tag{A6}$$

So Eqs. (A2b) and (A3) may be written as a system of equations,

$$(E_\mu-E)u_{\mu,n}+\frac{E_\mu}{E}\sum_{k_\perp} t_{k_\perp}^{\mu,n}\frac{2\hbar c|k_\perp|}{E+\hbar c|k_\perp|}\,u_{k_\perp}=0, \tag{A7a}$$

$$(\hbar c|k_\perp|-E)u_{k_\perp}+\sum_{\mu,n}(t_{k_\perp}^{\mu,n})^*\frac{2E_\mu}{E^2-E_\mu^2}\times\sum_{k_\perp} t_{k'_\perp}^{\mu,n}\frac{2c|k'_\perp|}{E+\hbar c|k'_\perp|}\,u_{k'_\perp}=0. \tag{A7b}$$

Substituting for the last sum in Eq. (A7b) its expression from Eq. (A7a) we transform Eqs. (A7a) and (A7b) to the form

$$(E_\mu-E)u_{\mu,n}+\frac{E_\mu}{E}\sum_{k_\perp} t_{k_\perp}^{\mu,n}\frac{2\hbar c|k_\perp|}{E+\hbar c|k_\perp|}\,u_{k_\perp}=0, \tag{A8a}$$

$$(\hbar c|k_\perp|-E)u_{k_\perp}+\sum_{\mu,n}(t_{k_\perp}^{\mu,n})^*\frac{2E}{E+E_\mu}\,u_{\mu,n}=0. \tag{A8b}$$

Substitution of $u_{k_\perp}$ from Eq. (A8b) to Eq. (A8a) yields the equation for $u_{\mu,n}$,

$$(E_\mu-E)u_{\mu,n}+2E_\mu\sum_{k_\perp} t_{k_\perp}^{\mu,n}\frac{2\hbar c|k_\perp|}{E^2-\hbar c^2k_\perp^2}\sum_{\mu',n'}(t_{k_\perp}^{\mu',n'})^*\times\frac{1}{E+E_{\mu'}}\,u_{\mu',n'}=0. \tag{A9}$$

For an isolated exciton band, the lowest singlet exciton in antracen, for example, we may take into account only one exciton band $\mu=\mu'=0$. Denoting $u_{\mu=0,n}\equiv u_n$, we obtain

$$(E^2-E_0^2)u_n=\sum_{n'}\left[\frac{8\pi E_0E^2|\mathbf{P}_0|^2M}{V}\sum_{k_\perp}\frac{e^{ik_\perp a(n-n')}}{E^2-\hbar^2c^2k_\perp^2}\right]u_{n'}. \tag{A10}$$

The transition from the sum to an integral is the following:

$$\frac{2\pi M}{V}\sum_{k_\perp}\to\frac{1}{a^2}\int dk_\perp. \tag{A11}$$

So the equation for u_n takes the form

$$(E^2-E_0^2)u_n=\frac{4E_0E^2|\mathbf{P}_0|^2}{a^2}\times\sum_{n'}\left[\int_{-\infty}^{+\infty}dk_\perp\frac{e^{ik_\perp a(n-n')}}{E^2-\hbar^2c^2k_\perp^2+i\eta}\right]u_{n'}. \tag{A12}$$

We seek decaying polariton states which correspond to complex energy in Eq. (A12) $E=E'-iE''$, $E'>0$, $E''>0$. The infinitesimal $\eta\to+0$ shows the directions of bypassing the poles: $k_\perp=-(E'-iE'')/\hbar c$—from above, $k_\perp=(E'-iE'')/\hbar c$—from below. Such a way of bypassing is determined by the form of the Green function of the photon field.

Performing the integration in Eq. (A12) yields the final equation for u_n,

$$(E^2-E_0^2)u_n+i\Gamma^{(2)}E\sum_{n'=1}^{N}\exp\left(i\,\frac{Ea}{\hbar c}\,|n-n'|\right)u_{n'}=0,\qquad \Gamma^{(2)}\equiv\frac{4\pi|P_0|^2}{a^2}\frac{E_0}{\hbar c}. \tag{A13}$$

[1] J. Hopfield, Phys. Rev. **112**, 1555 (1958).
[2] V. M. Agranovich, Zh. Exp. Teor. Fiz. **37**, 430 (1959); Sov. Phys. JETP **10**, 307 (1960).
[3] V. M. Agranovich and O. A. Dubovsky, Pisma Zh. Exp. Teor. Fiz. **3**, 345 (1966); JETP Lett. **3**, 223 (1966).
[4] V. M. Agranovich, *The Theory of Excitons* (Nauka, Moscow, 1968) (in Russian).
[5] Ya. Aaviksoo, Ya. Lippmaa, and T. Reinot, Opt. Spectrosc. **62**, 706 (1987).
[6] B. Devead, F. Clerot, N. Roy, K. Satzke, B. Sermage, and D. S. Katzer, Phys. Rev. Lett. **67**, 2355 (1991).
[7] K. L. Kliever and R. Fuchs, Phys. Rev. **150**, 573 (1966).
[8] M. R. Philpott, Chem. Phys. Lett. **30**, 387 (1975).
[9] J. Knoester, Phys. Rev. Lett. **68**, 654 (1992).
[10] J. Knoester, J. Lumin. **53**, 101 (1992).
[11] G. Björk, S. Pau, J. M. Jackobson, H. Cao, and Y. Yamamoto, Phys. Rev. B **52**, 17310 (1995).
[12] L. C. Andreani, Phys. Status Solidi B **188**, 29 (1995).
[13] V. M. Agranovich and V. L. Ginsburg, *Crystal Optics with Spatial Dispersion and Excitons* (Springer, Berlin, 1984).
[14] M. I. Podgoretsky and M. I. Roysen, Zh. Exp. Teor. Fiz. **39**, 1473 (1960); JETP **39**, 1473 (1960).